Article

# A Flexible Coordination Polymer Crystal Providing Reversible Structural and Magnetic Conversions

Wakako Kaneko, Masaaki Ohba, and Susumu Kitagawa

*J. Am. Chem. Soc.*, **2007**, 129 (44), 13706-13712• DOI: 10.1021/ja074915q • Publication Date (Web): 11 October 2007



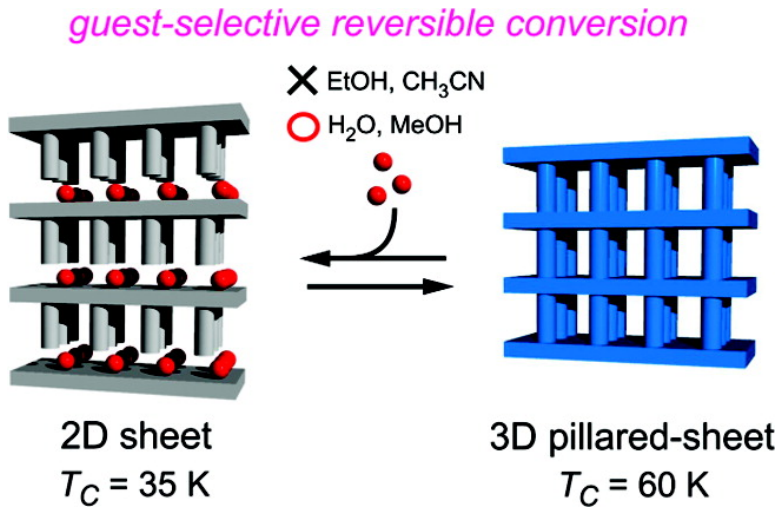

J|A|C|S
ARTICLES
Published on Web 10/11/2007

# A Flexible Coordination Polymer Crystal Providing Reversible Structural and Magnetic Conversions

Wakako Kaneko, Masaaki Ohba,* and Susumu Kitagawa*

*Contribution from the Department of Synthetic Chemistry and Biological Chemistry, Graduate School of Engineering, Kyoto University, Katsura, Nishikyo-ku, Kyoto 615-8510, Japan*

Received July 4, 2007; E-mail: ohba@sbchem.kyoto-u.ac.jp; kitagawa@sbchem.kyoto-u.ac.jp

***Abstract:*** Structural flexibility is a remarkable characteristic of coordination polymers and significant for the attainment of environmental responsivity. We have prepared a 2D cyanide-bridged $Mn^{II}Cr^{III}$ coordination polymer, $[Mn(NNdmenH)(H_2O)][Cr(CN)_6]\cdot H_2O$ (**1**; NNdmen = *N*,*N*-dimethylethylenediamine), with sophisticatedly arranged removable water coligands. The compound clearly showed a reversible single-crystal-to-single-crystal transformation between the 2D sheet and a 3D pillared-sheet framework of dehydrated $[Mn(NNdmenH)][Cr(CN)_6]$ (**1a**). The structural change was reversible and accompanied with generation/cleavage of CN−Mn bonds between 2D sheets by dehydration/hydration. Compounds **1** and **1a** also exhibited a ferrimagnetic ordering at 35.2 and 60.4 K, respectively, and the magnetic characteristics were reversibly converted by guest adsorption/desorption. In addition, the dehydrated **1a** demonstrated a size-selective solvent adsorption linking chemi- and physisorption processes and shrinkage/expansion of its framework. The flexible magnetic framework incorporating removable coligands delivered multifunctions with chemical response.

## Introduction

Reversible structural conversion is one of the key functions for preparing environmentally responsive materials that show specific outputs to external stimuli, e.g., light, heat, pressure, guest, etc.[1−4] How can we construct such a convertible structure? Much effort has been devoted to establish a rational design for such structures, but it is still a challenging issue, especially producing reversibility.[5−10]

Coordination polymers (CPs) are among the promising compounds for the achievement of reversible structural conversions because they naturally provide structural flexibility as an inherent characteristic of coordination bonds.[11−14] In addition, CPs can combine various components, e.g., bridging ligand, metal ion, coligand, etc., with sophisticated design of their frameworks, which is expected to be a platform for environmentally responsive products. Above all, porous coordination polymers (PCPs) are the most favorable candidates because their large and versatile pores allow not only expansion/shrinkage of their framework but also generation/cleavage of coordination bonds associated with guest adsorption/desorption.[15−26]

To combine the physical and porous properties, the PCPs exhibiting ordered magnetism, so-called porous magnets, have been prepared.[27−36] Guest adsorption/desorption act as chemical

(1) Irie, M. *Chem. Rev.* **2000**, *100*, 1685.
(2) Halder, G. J.; Kepert, C. J.; Moubaraki, B.; Murray, K. S.; Cashion. J. D. *Science* **2002**, *298*, 1762.
(3) Kitaura, R.; Seki, K.; Akiyama, G.; Kitagawa, S. *Angew. Chem. Int. Ed.* **2003**, *42*, 428.
(4) Maji, T. K.; Matsuda, R.; Kitagawa, S. *Nature Mater.* **2007**, *6*, 142.
(5) Matsumoto, A.; Odani, T. *Macromol. Rapid Commun.* **2001**, *22*, 1195.
(6) Hu, C.; Englert, U. *Angew. Chem., Int. Ed.* **2005**, *44*, 2281.
(7) Zhang, J.-P.; Lin, P.-P.; Zhang, W.-X.; Chen, X.-M. *J. Am. Chem. Soc.* **2005**, *127*, 14162.
(8) Chu, Q.; Swenson, D. C.; MacGillivray, L. R. *Angew. Chem., Int. Ed.* **2005**, *44*, 3569.
(9) Varshney, D. B.; Gao, X.; Friščić, T.; MacGillivray, L. R. *Angew. Chem., Int. Ed.* **2006**, *45*, 646.
(10) Eubank, J. F.; Kravtsov, V. C.; Eddaoudi, M. *J. Am. Chem. Soc.* **2007**, *129*, 5820.
(11) Yaghi, O. M.; O'Keeffe, M.; Ockwig, N. W.; Chae, H. K.; Eddaoudi, M.; Kim, J. *Nature* **2003**, *423*, 705.
(12) Hosseini, M. W. *Coord. Chem. Rev.* **2003**, *240*, 157.
(13) Kitagawa, S.; Kitaura, R.; Noro, S.-i. *Angew. Chem., Int. Ed.* **2004**, *43*, 2334.
(14) Férey, G.; Mellot-Dranznieks, C.; Serre, C.; Millange, F.; Dutour, J.; Surblé, S.; Margiolaki, I. *Science* **2005**, *309*, 2040.
(15) Mäkinen, S. K.; Melcer, N. J.; Parvez, M.; Shimizu, G. K. H. *Chem. Eur.—J.* **2001**, *7*, 5176.
(16) Uemura, K.; Kitagawa, S.; Kondo, M.; Fukui, K.; Kitaura, R.; Chang, H.-C.; Mizutani, T. *Chem.—Eur. J.* **2002**, *8*, 3586.
(17) Suh, M. P.; Ko, J. W.; Choi, H. J. *J. Am. Chem. Soc.* **2002**, *124*, 10976.
(18) Rosseinsky, M. J. *Microporous Mesoporous Mater.* **2004**, *73*, 15.
(19) Lee, E. Y.; Suh, M. P. *Angew. Chem., Int. Ed.* **2004**, *43*, 2798.
(20) Matsuda, R.; Kitaura, R.; Kitagawa, S.; Kubota, Y.; Kobayashi, T. C.; Horike, S.; Takata, M. *J. Am. Chem. Soc.* **2004**, *126*, 14063.
(21) Maji, T. K.; Mostafa, G.; Matsuda, R.; Kitagawa, S. *J. Am. Chem. Soc.* **2005**, *127*, 17152.
(22) Takaoka, K.; Kawano, M.; Tominaga, M.; Fujita, M. *Angew. Chem., Int. Ed.* **2005**, *44*, 2151.
(23) Takamizawa, S.; Nakata, E.-i.; Akatsuka, T. *Angew. Chem., Int. Ed.* **2006**, *45*, 2216.
(24) Takamizawa, S.; Kojima, K.; Akatsuka, T. *Inorg. Chem.* **2006**, *45*, 4580.
(25) Brandshaw, D.; Warren, J. E.; Rosseinsky, M. J. *Science* **2007**, *315*, 977.
(26) Heo, J.; Jeon, Y.-M.; Mirkin, C. A. *J. Am. Chem. Soc.* **2007**, *129*, 7712.
(27) Coronado, E.; Galán-Mascarós, J. R.; Gómez-García, C. J.; Laukhin, V. *Nature* **2000**, *408*, 447.
(28) Maspoch, D.; Ruiz-Molina, D.; Wurst, K.; Domingo, N.; Cavalliano, M.; Biscarini, F.; Tejada, J.; Rovira, C.; Veciana, J. *Nat. Mater.* **2003**, *2*, 190.
(29) Férey, G. *Nat. Mater.* **2003**, *2*, 136.
(30) Ohkoshi, S.; Arai, K.; Sato, Y.; Hashimoto, K. *Nat. Mater.* **2004**, *3*, 857.
(31) Wang, Z.; Zhang, B.; Fujiwara, H.; Kobayashi, H.; Kurmoo, M. *Chem. Commun.* **2004**, 416.
(32) Kurmoo, M.; Kumagai, H.; Chapman, K. W.; Kepert, C. J. *Chem. Commun.* **2005**, 3012.
(33) Cui, H.; Wang, Z.; Takahashi, K.; Okano, Y.; Kobayashi, H.; Kobayashi, A. *J. Am. Chem. Soc.* **2006**, *128*, 15074.
(34) Ohkoshi, S.; Tsunobuchi, Y.; Takahashi, H.; Hozumi, T.; Shiro, M.; Hashimoto, K. *J. Am. Chem. Soc.* **2007**, *129*, 3084.
(35) Yanai, N.; Kaneko, W.; Yoneda, K.; Ohba, M.; Kitagawa, S. *J. Am. Chem. Soc.* **2007**, *129*, 3496.


**10.1021/ja074915q CCC: $37.00** 

stimuli in the CP magnets' (CPMs') framework and provide structural and magnetic modulation. Here, the single-crystal-to-single-crystal (SCSC) transformation is particularly important for gaining insights into the correlation between structure and magnetic properties. However, there are still only a few examples that deliver simultaneous and reversible SCSC and magnetic conversion. To achieve this aim, we have focused on the flexible open space between the 2D magnetic layers in CPMs, in which interlayer interaction plays a major role in controlling bulk magnetic properties and strongly correlates with the interlayer topology and separation.[37−41] In particular, structural conversion from 2D to 3D, accompanied by the generation of a new coordination bond, should result in major magnetic changes with interlayer shrinkage and volume reduction. Such a material would be applicable for environmental responsive molecular actuators, magnetic sensors, optical isolators using magneto-optical properties, and so on. A sophisticated molecular design is indispensable for such a structural conversion, whereas the SCSC conversion in 2D/3D frameworks is very few even in CPs so far.[42,43]

We have extensively studied and established a rational synthesis method for cyanide-bridged CPMs by the use of $[M(CN)_6]^{n-}$ and various organic coligands.[35,39,44−48] The reversible magnetic conversion has been achieved in some CPMs by the hydration/dehydration process, which highlighted that incorporating removable coligands in the CPMs' framework and flexible cyanide-bridged linkages are crucial factors to deliver the environmental responsivity.[34,35,48−51] In this paper, we report a 2D $Mn^{II}Cr^{III}$ ferrimagnet, $[Mn(NNdmenH)(H_2O)][Cr(CN)_6]\cdot H_2O$ (**1**) (NNdmen = *N*,*N*-dimethylethylenediamine), and an anhydrous 3D ferrimagnet, $[Mn(NNdmenH)][Cr(CN)_6]$ (**1a**). A reversible SCSC structural conversion is demonstrated between these novel compounds, producing magnetic modulation and size-selective guest adsorption. Removable water coligands that are elaborately arranged on $Mn^{II}$ sites play a key role for reversible opening/closing of their pores accompanied with generation/cleavage of coordination bonds.

## Experimental Section

**Syntheis of $[Mn(NNdmenH)(H_2O)][Cr(CN)_6]\cdot nH_2O$.** $MnCl_2\cdot 4H_2O$ (59 mg, 0.3 mmol) was dissolved in degassed water (10 mL) using a standard Schlenk apparatus. An aqueous solution (5 mL) of NNdmen (53 mg, 0.6 mmol) and an aqueous solution (5 mL) of $K_3[Cr(CN)_6]$ (65 mg, 0.2 mmol) were added to this solution in turn under Ar at room temperature. A small excess of NNdmen is useful to avoid immediate aggregation of $[Cr(CN)_6]^{3-}$ and $Mn^{2+}$ ions producing the related Prussian blue-type compound, $Mn^{II}_3[Cr^{III}(CN)_6]_2\cdot nH_2O$. The resulting turbid mixture was allowed to stand for over 2 weeks to obtain pale-green crystals of $[Mn(NNdmenH)(H_2O)][Cr(CN)_6]\cdot nH_2O$. They were separated, collected by suction filtration, washed with water, and dried in *vacuo*. All the operations for the synthesis were carried out in the dark to avoid the decomposition of $K_3[Cr(CN)_6]$. The number of lattice water molecules (*n*) fluctuated between one and two, depending on the state of preservation, which was confirmed by the elemental analysis, TGA, and the adsorption isotherm of $H_2O$. The composition was finally defined to be $[Mn(NNdmenH)(H_2O)][Cr(CN)_6]\cdot H_2O$ (**1**) by consideration of all results. Yield: 16 mg (19%). Elemental analysis (%) calcd for $C_{10}H_{19}N_8O_3CrMn$: C, 29.57; H, 4.71; N, 27.58. Found: C, 29.73; H, 4.31; N, 27.65 (see Table S2). Selected FT−IR data [$\nu_{CN}$/$cm^{-1}$] using KBr disk: 2155, 2131.

**Physical Measurements.** Elemental analysis of carbon, hydrogen, and nitrogen was carried out on a Flash EA 1112 series, Thermo Finnigan instrument. Infrared spectra were measured using KBr disks with a Perkin-Elmer Spectrum 2000 FT−IR system. Variable-temperature X-ray powder diffraction was carried out on a Rigaku RINT-2000 Ultima diffractometer with Cu Kα radiation. Thermogravimetric analyses were recorded on a Rigaku Thermo plus TG 8120 apparatus in the temperature range between 300 and 700 K under a nitrogen atmosphere at a heating rate of 1 K $min^{-1}$. TGA repeatability measurements were performed in the temperature range 303−373 K at heating and cooling rates of 5 K $min^{-1}$. The adsorption isotherms of $H_2O$, MeOH, EtOH, and $CH_3CN$ at 298 K were measured with BELSORP18 volumetric adsorption equipment from Bel Japan, Inc. The anhydrous sample (**1a**) was obtained by treatment under reduced pressure ($<10^{-2}$ Pa) at 373 K for more than 10 h. Magnetic measurements were carried out on a Quantum Design MPMS-XL5R SQUID susceptometer. Samples were put into a gelatin capsule, mounted inside straw, and then fixed to the end of the sample transport rod. Diamagnetic correction was made with the Pascal's constants. The molar magnetic susceptibility, $\chi_M$, was corrected for the diamagnetism of the constituent atoms. DC magnetic measurements were performed in the temperature range 2−300 K in an applied dc field of 500 Oe. AC magnetic measurements were performed in the frequency range 1−1000 Hz in an applied ac field of 3 Oe. Field dependences of magnetization were measured in the field range 0−50 kOe at 2 K.

**Crystal Structure Determination.** X-ray diffraction data of **1** and **1a** were collected on a Rigaku Mercury CCD system with graphite-monochromated Mo Kα radiation ($\lambda$ = 0.710 70 Å). A single crystal of **1** was mounted on a glass fiber with a thin coat of resin and kept at 243 K under flowing $N_2$. All the structures were solved by a standard direct method and expanded using Fourier techniques. Full-matrix least-squares refinements were carried out using teXsan with anisotropic thermal parameters for all non-hydrogen atoms.[52] All the hydrogen atoms were placed in the calculated positions and refined using a riding model.

Crystal data for $[Mn(NNdmenH)(H_2O)][Cr(CN)_6]\cdot H_2O$ (**1**) at 243 K: pale-green crystals, $C_{10}H_{17}CrMnN_8O_2$, $M_r$ = 388.23, monoclinic, space group $P2_1/n$ (No. 14), $Z$ = 4, $a$ = 7.681(3) Å, $b$ = 14.498(5) Å, $c$ = 16.598(6) Å, $\beta$ = 97.326(5)°, $V$ = 1833(1) $Å^3$, $D_{calcd}$ = 1.407 g $cm^{-3}$, $\mu$(Mo Kα) = 12.98 $cm^{-1}$. $R$ = 0.076, $R_w$ = 0.079 (all data) and $R_1$ = 0.061 ($I > 2.0\sigma(I)$). Crystal data for $[Mn(NNdmenH)][Cr(CN)_6]$ (**1a**) at 343 K: pale-green crystals, $C_{10}H_{13}CrMnN_8$, $M_r$ = 352.20, monoclinic, space group $P2_1/c$ (No. 14), $Z$ = 4, $a$ = 7.85(1) Å, $b$ = 14.31(3) Å, $c$ = 12.97(2) Å, $\beta$ = 90.10(3)°, $V$ = 1456.2(4) $Å^3$, $D_{calcd}$ = 1.606 g $cm^{-3}$, $\mu$(Mo Kα) = 16.15 $cm^{-1}$. $R$ = 0.155, $R_w$ = 0.115 ($I$


(36) Cheng, X.-N.; Zhang, W.-X.; Lin, Y.-Y.; Zheng, Y.-Z.; Chen, X.-M. *Adv. Mater.* **2007**, *19*, 1494.
(37) Nakatani, K.; Bergerat, P.; Codjovi, E.; Mathoniere, C.; Pei, Y.; Kahn, O. *Inorg. Chem.* **1991**, *30*, 3978.
(38) Turner, S.; Kahn, O.; Rabardel, L. *J. Am. Chem. Soc.* **1996**, *118*, 6428.
(39) Ohba, M.; Ōkawa, H.; Fukita, N.; Hashimoto, Y. *J. Am. Chem. Soc.* **1997**, *119*, 1011.
(40) Fujita, W.; Awaga, K. *J. Am. Chem. Soc.* **1997**, *119*, 4563.
(41) Shimizu, H.; Okubo, M.; Nakamoto, A.; Enomoto, M.; Kojima, N. *Inorg. Chem.* **2006**, *45*, 10240.
(42) Niel, V.; Thompson, A. L.; Muñoz, M. C.; Galet, A.; Goeta, A. E.; Real, J. A. *Angew. Chem., Int. Ed.* **2003**, *42*, 3760.
(43) Kepert, C. J. *Chem. Commun.* **2006**, 695.
(44) Ohba, M.; Ōkawa, H. *Coord. Chem. Rev.* **2000**, *198*, 313.
(45) Ohba, M.; Maruono, N.; Ōkawa, H.; Enoki, T.; Latour, J. M. *J. Am. Chem. Soc.* **1994**, *116*, 11566.
(46) Inoue, K.; Kikuchi, K.; Ohba, M.; Ōkawa, H. *Angew. Chem., Int. Ed.* **2003**, *42*, 4810.
(47) Kaneko, W.; Kitagawa, S.; Ohba, M. *J. Am. Chem. Soc.* **2007**, *129*, 248.
(48) Usuki, N.; Ohba, M.; Ōkawa, H. *Bull. Chem. Soc. Jpn.* **2002**, *75*, 1693.
(49) Miyasaka, H.; Matsumoto, N.; Re, N.; Gallo, E.; Ōkawa, H. *Inorg. Chem.* **1997**, *36*, 670.
(50) Larionova, J.; Chavan, S. A.; Yakhmi, J. V.; Frøystein, A. G.; Sletten, J.; Sourisseau, C.; Kahn, O. *Inorg. Chem.* **1997**, *36*, 6374.
(51) Miyasaka, H.; Ieda, H.; Matsumoto, N.; Re, N.; Crescenzi, R.; Floriani, C. *Inorg. Chem.* **1998**, *37*, 255.
(52) *teXsan: Crystal Structure Analysis Package*; The Molecular Structure Corporation: Woodlands, TX (1985 and 1992).

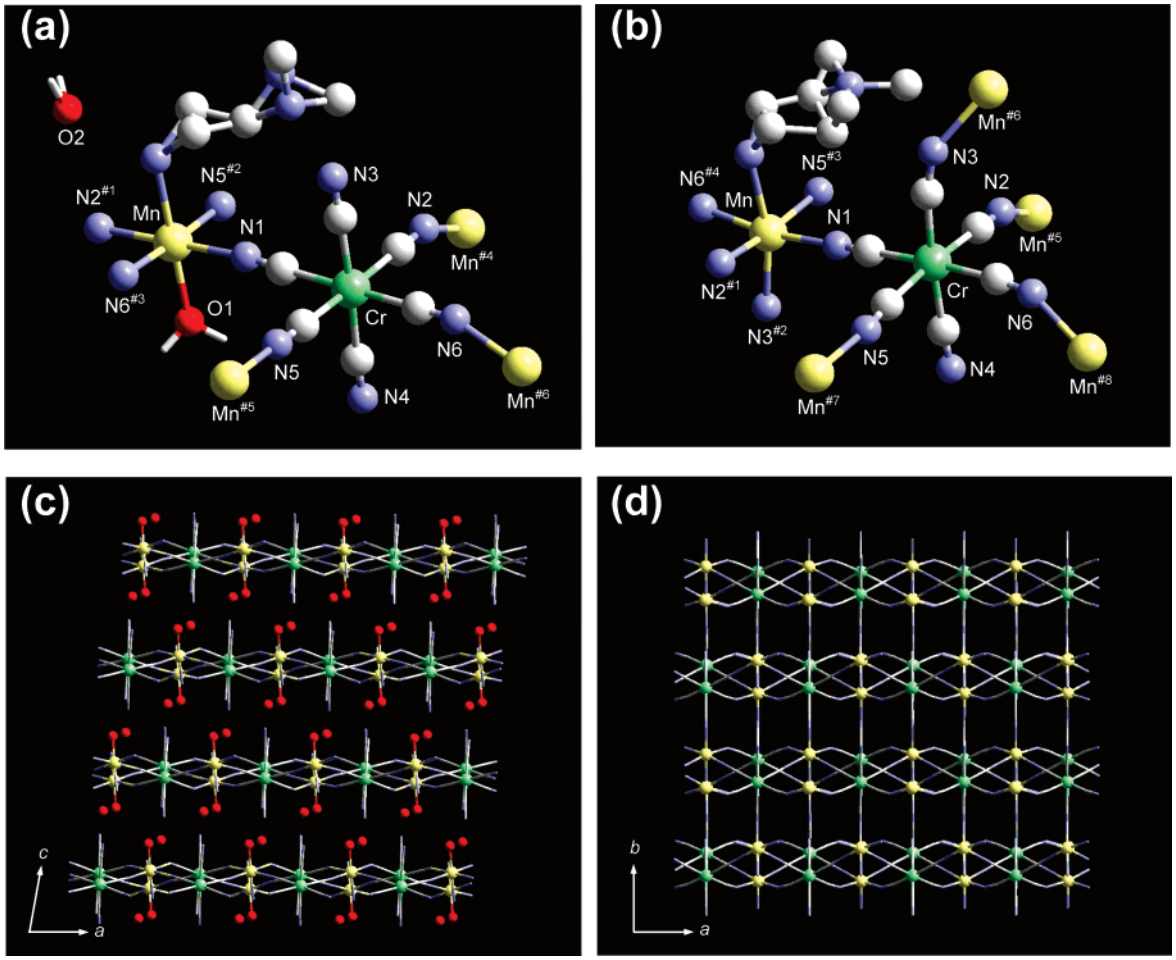


***Figure 1.*** Asymmetric unit of $[Mn(NNdmenH)(H_2O)][Cr(CN)_6]\cdot H_2O$ (**1**; a) and $[Mn(NNdmenH)][Cr(CN)_6]$ (**1a**; b) with the atom numbering scheme and projections of the 2D sheet of **1** onto the *ac* plane (c) and the 3D network of **1a** onto the *ab* plane (d). NNdmenH coligands are omitted for clarity in (c) and (d). Atoms: Mn (yellow), Cr (green), N (blue), O (red), C (gray).

$> 0.5\sigma(I)$) and $R_1 = 0.096$ ($I > 2.0\sigma(I)$). The symmetry operations: for **1** #1: $^1/_2 - x, ^1/_2 + y, ^1/_2 - z$; #2: $-1 + x, y, z$; #3: $^3/_2 - x, ^1/_2 + y, ^1/_2 - z$; #4: $^1/_2 - x, -^1/_2 + y, ^1/_2 - z$; #5: $1 + x, y, z$; #6: $^3/_2 - x, -^1/_2 + y, ^1/_2 - z$; #7: $-^1/_2 + x, ^1/_2 - y, ^1/_2 - z$; #8: $-^1/_2 + x, ^1/_2 - y, -^1/_2 + z$. For **1a** #1: $x, ^3/_2 - y, -^1/_2 + z$; #2: $1 - x, -^1/_2 + y, ^1/_2 - z$; #3: $1 + x, y, z$; #4: $1 + x, ^3/_2 - y, -^1/_2 + z$; #5: $x, ^3/_2 - y, ^1/_2 + z$; #6: $1 - x, ^1/_2 + y, ^1/_2 - z$; #7: $1 - x, y, z$; #8: $-1 + x, ^3/_2 - y, ^1/_2 + z$.

## Results and Discussions

**Crystal Structure.** $[Mn(NNdmenH)(H_2O)][Cr(CN)_6]\cdot nH_2O$ was obtained as pale-green efflorescent crystals by the reaction of $K_3[Cr(CN)_6]$, $MnCl_2\cdot 4H_2O$, and coligand (NNdmen) in a deoxygenated aqueous solution at room temperature (Figure S1). The crystal structures of $[Mn(NNdmenH)(H_2O)][Cr(CN)_6]\cdot H_2O$ (**1**) and anhydrous form **1a** were determined by X-ray crystallographic analyses. To prepare the anhydrous form **1a**, the crystal of **1** was slowly and carefully heated to 343 K on the glass fiber, and then the data were collected at 343 K. Selected bond distances and angles of **1** and **1a** are listed in Table S1.

The asymmetric unit of **1** consists of $[Mn(NNdmenH)(H_2O)]^{3+}$ cation, $[Cr(CN)_6]^{3-}$ anion, and a lattice water molecule (Figure 1a). Both $Mn^{II}$ and $Cr^{III}$ ions are in a pseudo-octahedral geometry. Four cyano nitrogen atoms (N1, N2, N5, and N6) in the equatorial position of $[Cr(CN)_6]^{3-}$ coordinate to adjacent $Mn^{II}$ ions to form a 2D corrugated sheet structure on the *ab* plane (Figures 1c, 2a). The 2D corrugated sheets form 1D channels segmented by NNdmen along the *a*-axis. The averaged Mn−N bond distance and Mn−N−C bond angles are 2.205 Å and 166.0°, respectively. Bent Cr−CN−Mn linkages (C2−N2−$Mn^{\#4}$ = 151.2(4)°, C6−N6−$Mn^{\#6}$ = 161.0(4)°) form the corrugated sheet. A water molecule is located at the axial positions of the octahedral $Mn^{II}$ ion as monodentate coligands. An NNdmen is protonated and occupied the other axial position of $Mn^{II}$ as a cationic monodentate ligand in two disordered configurations. The coordinated water coligand forms bidirectional hydrogen bonds with a lattice water ($O1\cdots O2^{\#4} = 2.829$ Å) and a coordination-free cyano nitrogen atom (N3) in the next sheet ($O1\cdots N3^{\#7} = 2.753$ Å). The lattice water molecules reside in the space between the sheets forming bidirectional hydrogen bonds with a water coligand and a coordination-free cyano nitrogen atom (N4) in the next sheet ($N4^{\#8}\cdots O2 = 2.836$ Å). Only one lattice water was crystallographically determined, which suggests that the other lattice water was partially released and disordered under $N_2$ flow conditions. The shortest intrasheet Mn···Mn, Cr···Cr, and Mn···Cr distances are 7.299, 7.378, and 5.239 Å, and those of the intersheet distances are 8.917, 8.133, and 7.378 Å, respectively. The topology between the sheets is adjusted by the hydrogen bond between the water coligand and the coordination-free cyanide group (N3).

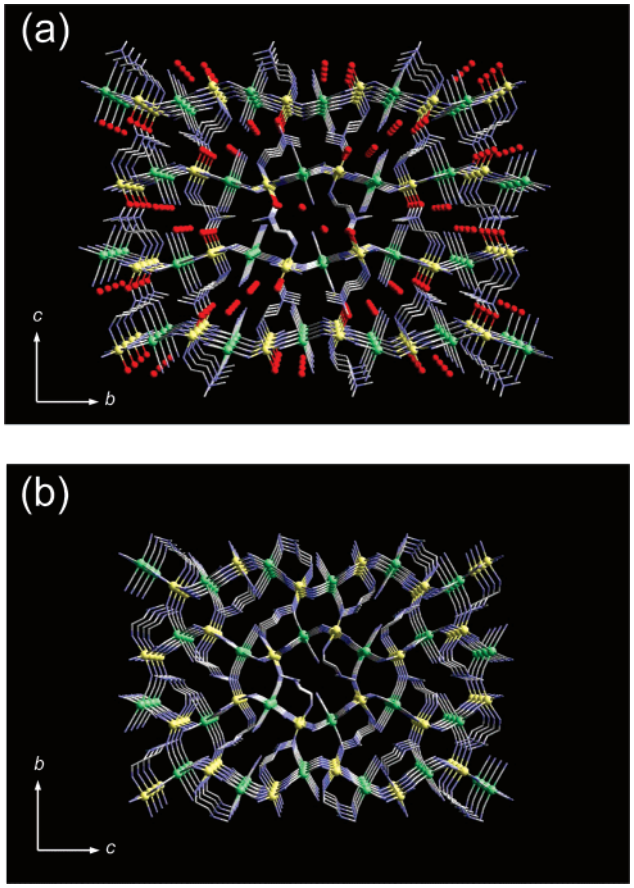


***Figure 2.*** Projections of **1** onto the *bc* plane (a) and **1a** onto the *bc* plane (b).

The crystal structure of **1a** was solved in space group $P2_1/c$, which is different from the case for **1** ($P2_1/n$). The *b* and *c* axes in **1** correspond to the *c* and *b* axes in **1a**, respectively. The asymmetric unit of **1a** consists of $[Mn(NNdmenH)]^{3+}$ cation and $[Cr(CN)_6]^{3-}$ anion with no lattice and coordinated water molecules (Figure 1b). The 2D corrugated sheet is formed on the *ac* plane in a similar way to **1** (Figures 1d, 2b). The water coligand on $Mn^{II}$ in **1** was removed by heating, and the cyano nitrogen ($N3^{\#2}$) of $[Cr(CN)_6]^{3-}$ on the adjacent sheet directly bound to the $Mn^{II}$ ion, instead of the water coligand. The intersheet Cr−C3−N3−Mn linkages construct a 3D pillared-sheet framework in the lattice (Figure 2b). The average equatorial Mn−N bond distances and Mn−N−C angles are 2.212 Å and 163.4°, respectively. The topology of the 2D sheet in **1** was carried on into **1a**. The shortest intrasheet Mn···Mn, Cr···Cr, and Mn···Cr distances are 6.958, 6.700, and 5.199 Å, and the shortest intersheet distances are 7.164, 7.358, and 5.070 Å, respectively. The cell volume of **1a** was reduced by ca. 20% compared with that of **1** with remarkable shrinking in the *bc* plane. It is remarkable that the bond angle of Cr−C3−N3 was far from being linear (169.4(9)°), which means a structural strain around $[Cr(CN)_6]^{3-}$. The new intersheet $Mn^{\#6}$−N3−C3 linkage is also bent with a bond angle of 146.6(8)°. The bond angles of intrasheet $Mn^{\#5}$−N2−C2 (155.0(10)°) and $Mn^{\#8}$−N6−C6 (154.4-(9)°) linkages became larger than those of **1**. These three bent Cr−CN−Mn linkages cause shrinkage in the *bc* plane and form a narrow 1D channel based on a highly distorted $Mn_2Cr_2$ quadrangular gate (0.8 × 1.6 Å$^2$ based on van der Waals radii) along the *a*-axis. These structural strains, flexible Cr−CN−Mn linkages, and the existence of a narrow channel would be crucial factors for the restoration to a 2D sheet of **1** mentioned below. Although the 1D channel is too narrow to admit guest molecules, it is a key ingredient for guest-induced structural transformation accompanied with breaking the Mn−N3 bond (opening the gate). In addition, the single crystal **1a** gives the same crystal parameter of **1** after rehydration (**1b**).

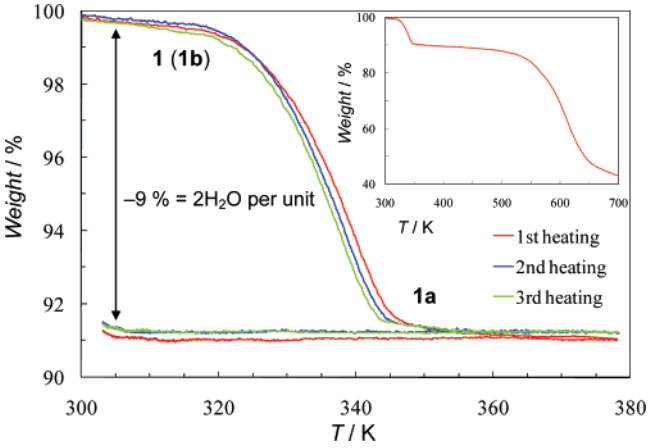


***Figure 3.*** TGA repeatability measurements of **1**. The sample of **1** was heated from 298 to 373 K at 5 K/min, maintained for 1 h, then cooled to 298 K at 5 K/min, and exposed to the atmosphere for 2 h. These processes were performed three times. Insert is the one-way heating process of **1** from 300 to 700 K at 1 K/min.

**Structural Stability.** The TGA curve indicated a slight weight loss around room temperature under $N_2$ flow (Figure 3), which suggests that one of the lattice water molecules per unit can be easily removed under low humidity conditions, consistent with the X-ray crystallographic results. In the heating process from 298 K, the TGA curve showed a weight loss of ca. 8.8% around 343 K, which substantially corresponds to one lattice water and one water coligand per unit. Therefore, the number of lattice water molecules of **1** is taken to be one, because all measurements were carried out under $N_2$ or He (low humidity conditions). No additional weight loss was observed while the sample was maintained at 373 K for 1 h. The anhydrous **1a** showed no weight increase on cooling to 298 K under $N_2$. When **1a** was exposed in the open air or to water vapor, it immediately reproduced the initial weight of **1** almost completely. Here, the rehydrated form is defined as **1b** for convenience. **1b** was converted to **1a** again by heating to 373 K. The reversibility between **1b** and **1a** was confirmed many times. The anhydrous **1a** was stable up to 500 K and decomposed on further heating (Figure 3, insert). To confirm the simultaneous structural transformation with the dehydration/hydration process and the framework stability of **1**, variable-temperature X-ray powder diffraction (VT-XRPD) was performed under vacuum in the temperature range 303−373 K (Figure 4). The pattern of the as-synthesized **1** showed good agreement with the simulated pattern based on its X-ray crystal structure. Upon heating, the pattern suddenly changed between 333 and 343 K, which agrees with the TGA results. The pattern of the anhydrous form was consistent with the simulated pattern generated by the crystallographic data of **1a**. This 3D network of **1a** was maintained upon cooling to 303 K under vacuum. By exposure to air or water vapor at 303 K, **1a** immediately reproduced the same XRPD pattern as **1**. The TGA and VT-XRPD results clearly demonstrate a repetitive structural conver-

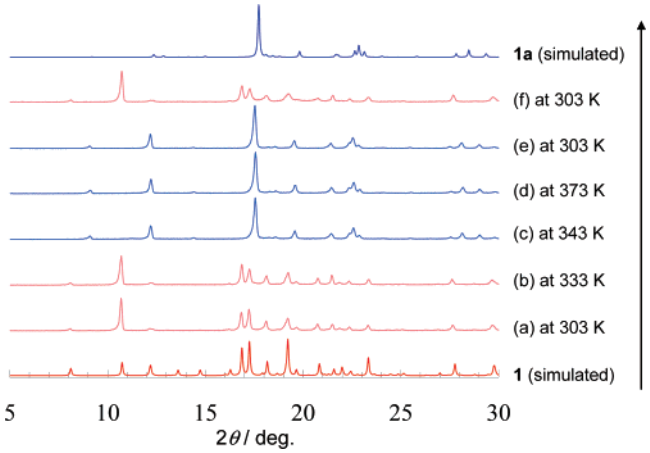


***Figure 4.*** Temperature dependence of the XRPD patterns for **1**. Crystalline **1** was heated from 303 K (a) to 373 K (d) and cooled to 303 K (e) under vacuum conditions, then exposed to the atmosphere at 303 K (f). Simulated patterns generated by X-ray crystallographic results for **1** and **1a** are also presented.

sion between 2D $[Mn(NNdmenH)(H_2O)][Cr(CN)_6]\cdot H_2O$ (**1**, **1b**) and 3D $[Mn(NNdmenH)][Cr(CN)_6]$ (**1a**) by the dehydration/hydration process.

**Guest Adsorption.** The adsorption isotherms of various solvent vapors on anhydrous **1a** were measured at 298 K (Figure 5a). The profile of water adsorption shows a steep increase in the low relative pressure ($P/P_0$) region, which suggests a high affinity of **1a** for water. The saturated amount of water adsorption of 2.3 mol/mol in the measurement time scale (equilibrium time = 800 s) agrees with the results of TGA and EA (Table S2), that is, one water coligand and one lattice water. The desorption profile showed a large hysteresis, because of restoration of the 2D structure. In the low relative pressure region, a small and reproducible step was observed at $P/P_0$ = 0.08, where the adsorption amount corresponds to one water molecule per unit (Figure 5b). From the structural insights gained for **1** and **1a**, it is assumed that the framework of **1a** provides two kinds of water sorption sites, namely, (1) a chemisorption site on the $Mn^{II}$ ion and (2) a vacancy for physisorption between the 2D sheets. By the above considerations, the anomaly at $P/P_0$ = 0.08 should reflect the different adsorption types. From the structural aspects, the narrow 1D channels that are formed by Cr−C2N2−Mn, Cr−C3N3−Mn, and Cr−C6N6−Mn linkages in **1a** can act as an accessible gate to $Mn^{II}$ sites upon breaking the Mn−N3 bond and expanding the intersheet space. From these results, it is a reasonable deduction that adsorption in the region lower than $P/P_0$ = 0.08 occurred at the chemisorption site of (1) and the subsequent adsorption is attributed to physisorption at (2) as lattice water. The isotherm was analyzed using the Dubinin−Radushkevich (DR) equation to estimate the zeolitic property of **1a**.[53,54] The DR plot of **1a** showed a linear relationship in the low $P/P_0$ range, which establishes the strong affinity for water (Figure S2).

In the case of MeOH adsorption, the profile showed a gradual increase in the low $P/P_0$ region, an induction pressure of $P/P_0$ = 0.6 and absorption of ca. 1.5 mol of MeOH at $P/P_0$ = 0.95. This behavior demonstrates that **1a** undergoes the same structural change to the water adsorption. Compared with the small water molecule, the larger MeOH molecule needs a higher induction pressure because of the narrow accessible space of **1a**. In the desorption process, one MeOH remained per unit even in the low $P/P_0$ region, which suggests that the MeOH molecule can also access and coordinate to the Mn ion with breaking of the Mn−N3 bond. It is also noted that **1a** showed negligible EtOH and $CH_3CN$ adsorption in the time scale (equilibrium time = 600−1200 s) at 298 K. This is because these adsorbates are too large to proceed into the void space. In addition, (i) the low affinity of the cyano nitrogen donation to manganese(II) compared with oxygen and (ii) the rigid linear shape of $CH_3CN$ are also crucial reasons for the $CH_3CN$ shedding.

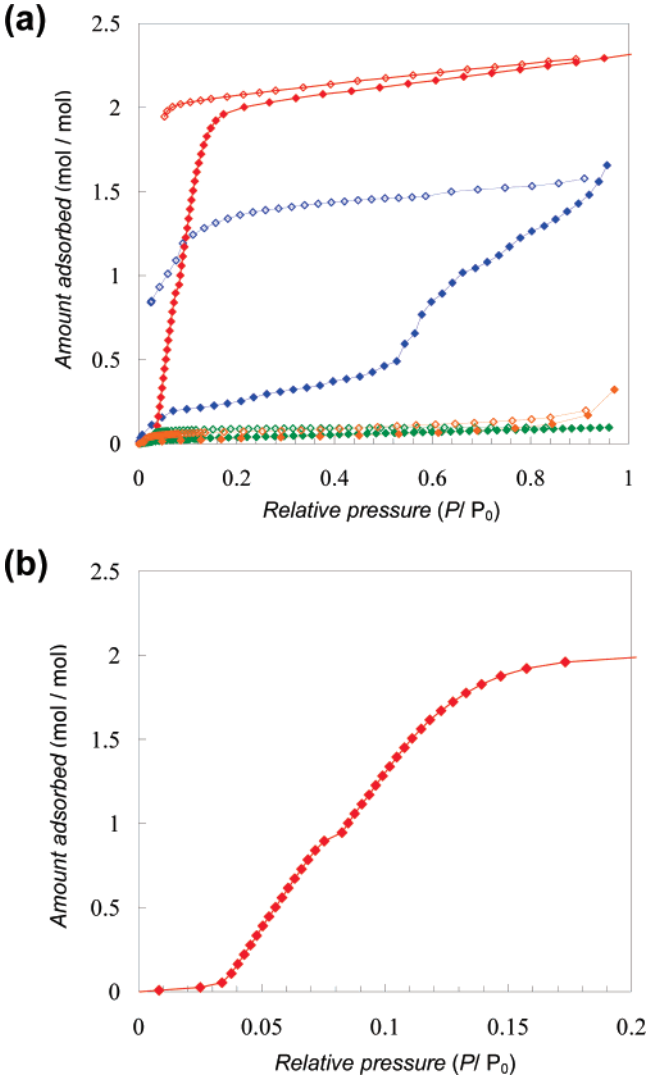


***Figure 5.*** Adsorption and desorption isotherms for vapor adsorption in **1a**. (a) Water (red), MeOH (blue), EtOH (green), and $CH_3CN$ (orange) at 298 K in the relative pressure range from $10^{-3}$ to 1.0 (■ and □ express adsorption and desorption process, respectively). $P/P_0$ is the relative pressure, where saturated vapor pressures, $P_0$, at 298 K are 3.53 kPa for water, 16.94 kPa for MeOH, 7.87 kPa for EtOH, and 11.79 kPa for $CH_3CN$. (b) Expansion in the low relative pressure region for the water adsorption isotherm.

**Magnetic Properties.** To obtain insight into the structural transformation by magnetic information, we successively measured magnetic data of **1**, **1a**, and **1b** with the same samples. The sample was placed in a gelatin capsule, mounted inside

(53) Dubinin, M. M. *Chem. Rev.* **1960**, *60*, 235.
(54) Lin, X.; Blake, A. J.; Wilson, C.; Sun, X. Z.; Champness, N. R.; George, M. W.; Hubberstey, P.; Mokaya, R.; Schröder, M. *J. Am. Chem. Soc.* **2006**, *128*, 10745.

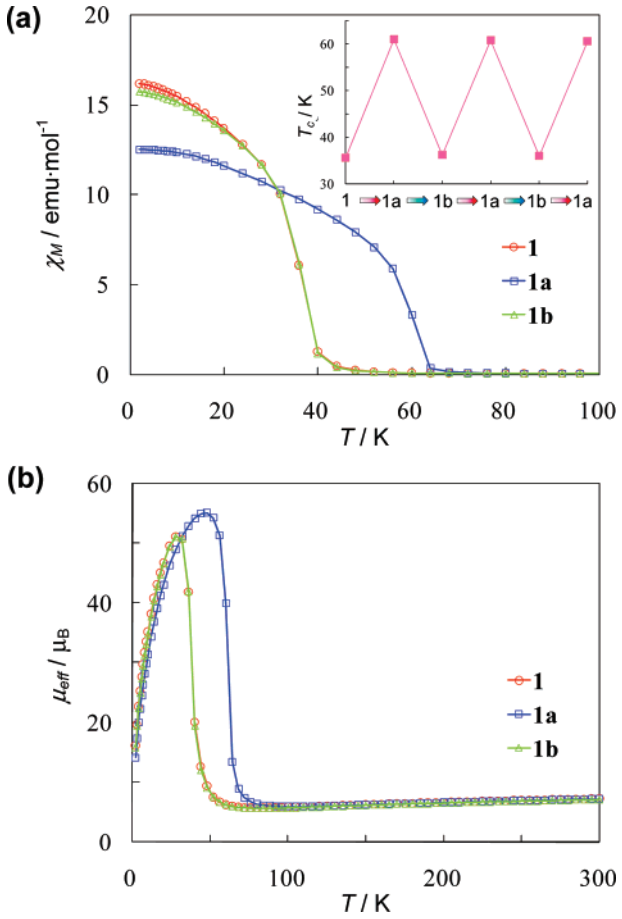


***Figure 6.*** (a) Temperature dependence of molar magnetic susceptibility $\chi_M$ for as-synthesized form **1** (red), dehydrated form **1a** (blue), and rehydrated form **1b** (green) in an applied dc field of 500 Oe. The insert demonstrates the reversible $T_C$ switching by dehydration/hydration treatments (red/blue arrows, respectively). (b) Temperature dependence of effective magnetic moment $\mu_{eff}$ for **1** (red), **1a** (blue), and **1b** (green).

straw, and then fixed to the end of the sample transport rod. Anhydrous **1a** was prepared by heating at 400 K for 7 h in the SQUID sample chamber after measurement of **1**. The released water from **1** was effectively purged from the sample space by vacuuming and He substitution at 400 K to measure the magnetic properties of **1a**. After measurement of **1a**, the capsulated sample was aerated sufficiently before being used for measurement as **1b**.

The dc magnetic susceptibilities of **1**, the anhydrous **1a**, and the rehydrated form **1b** are shown in the form of $\chi_M$ vs $T$ and $\mu_{eff}$ vs $T$ plots (Figure 6 and Table S3). The $\chi_M$ value per $Mn^{II}$-$Cr^{III}$ unit of **1** was 0.0217 emu·mol$^{-1}$ (7.22 $\mu_B$) at room temperature, which agrees well with the spin-only value (0.0208 emu·mol$^{-1}$, 7.07 $\mu_B$) expected for magnetically isolated $Mn^{II}$ ($S = {}^5/_2$) and $Cr^{III}$ ($S = {}^3/_2$) ions. The $\mu_{eff}$ value gradually decreased with decreasing temperature to reach a minimum value of 5.67 $\mu_B$ at 84 K, and then $\mu_{eff}$ increased rapidly below 50 K to a maximum value of 51.1 $\mu_B$ at 28 K. The $1/\chi_M$ vs $T$ plot in the temperature range of 300−150 K obeys the Curie−Weiss law with a Weiss constant $\theta$ of −164 K, which suggests the operation of an antiferromagnetic interaction between adjacent $Mn^{II}$ and $Cr^{III}$ ions through cyanide bridges. The rapid increase in $\mu_{eff}$ suggests a ferrimagnetic ordering, which was determined accurately as 35.2 K by the weak-field magnetization, the d$M$/d$T$ differential plot, and the ac magnetic susceptibility (Figures S3, S6). The out-of-phase signal of ac susceptibility ($\chi_M''$) clearly showed the magnetic ordering at 35.2 K and also indicated a secondary peak around 12 K. The behavior below $T_C$ reflects a change in magnetic domain structure.[55,56]

**1a** also showed a typical ferrimagnetic ordering at higher $T_C$ (60.4 K) than that of **1** (Figures S4, S7). The Weiss constant $\theta$ was calculated as −160 K in 300−150 K. AC susceptibilities of **1a** showed a single peak at 60 K and no anomaly was observed around 35 K, which clearly suggests that **1a** contains a single magnetic phase without contamination of **1**. The remarkable increase of $T_C$ in **1a** can be roughly explained by considering molecular field theory, which is expressed as eq 1[57,58]

$$T_C = 2(n_{Cr}n_{Mn})^{1/2}|J|\{S_{Cr}(S_{Cr}+1)S_{Mn}(S_{Mn}+1)\}^{1/2}/3k_B \quad (1)$$

where $n_{Cr}$ and $n_{Mn}$ mean the number of the nearest magnetic centers around Cr and Mn ions, respectively, $S_{Cr}$ and $S_{Mn}$ are the spin quantum numbers of the metals, $J$ is the exchange interaction constant, and $k_B$ is the Boltzmann constant. The increase of the number of the nearest magnetic centers $n$, that is, high dimensionality, is the effective factor for the increase in $T_C$ in **1a**; e.g., ($n_{Cr}$, $n_{Mn}$) = (5, 5) for **1a**, while ($n_{Cr}$, $n_{Mn}$) = (4, 4) for **1**. The absolute value of $|J|$ also strongly contributes to $T_C$, which is the product of overall magnetic interaction and represented as $(|J_{intra}|^2|J_{inter}|)^{1/3}$ for a 2D structure, while $J = J_{intra}$ for an ideal 3D structure, where $J_{intra}$ is the through-bond interaction and $J_{inter}$ is the through-space interaction, and $|J_{inter}| \ll |J_{intra}|$. However, compared with **1**, $|J_{intra}|$ in the 2D sheet of **1a** should be decreased because the Cr−CN−Mn linkages are remarkably bent, which means a decrease in the overlap integral between the d$\pi$ orbitals of the Cr and Mn ions. The intersheet Cr−C3N3−Mn linkage is also far from linear, which provides weak $J_{intra}$ but stronger than $J_{inter}$ in **1**. The structural strain provides a negative contribution to $T_C$. Therefore, the increase in $T_C$ in **1a** is the result of the overall contribution of the parameters $n_{Cr}$, $n_{Mn}$, and $J$.

After rehydration, it is worth emphasizing that the $\chi_M$ vs $T$ plot of **1b** almost fully traces the initial profile of **1**. The ac susceptibility results showed the generation of single-phase magnetic structure with $T_C$ = 35 K (Figures S5, S8). One of the major reasons for the difference between **1** and **1b** is a slight structural difference concerning the number of lattice waters, which would affect the propagation of the magnetic domain between the 2D sheets. Judging from the VT-XRPD and magnetic results, **1b** can be essentially identified as **1**, and the reversible interlocked structural and magnetic conversions were achieved. The reversible magnetic performance between **1a** and **1b** was confirmed repeatedly. (Figure 6a, inset).

The field dependence of the magnetization curves of **1** and **1a** at 2 K showed a rapid increase to saturate above 10 kOe (Figure S9). The saturation magnetization values per $Mn^{II}Cr^{III}$ unit at 50 kOe are 2.12 (**1**), 2.15 (**1a**), and 2.11 (**1b**) $N\beta$, which correspond to the value $S_T$ = 2/2 expected for antiferromagnetically coupled $Mn^{II}$ and $Cr^{III}$ ions with an average $g$ value of 2.17 (**1**), 2.19 (**1a**), and 2.17 (**1b**), respectively. The larger

(55) Salah, M. B.; Vilminot, S.; André, G.; Richard-Plouet, M.; Mhiri, T.; Takagi, S.; Kurmoo, M. *J. Am. Chem. Soc.* **2006**, *128*, 7972.
(56) Coronado, E.; Gómez-García, C.; Nuez, A.; Romero, F. M.; Waerenborgh, J. C. *Chem. Mater.* **2006**, *18*, 2670.
(57) Néel, L. *Annals Phys.* **1948**, *3*, 137.
(58) Kahn, O. *Molecular Magnetism*; VCH: Weinheim, 1993.

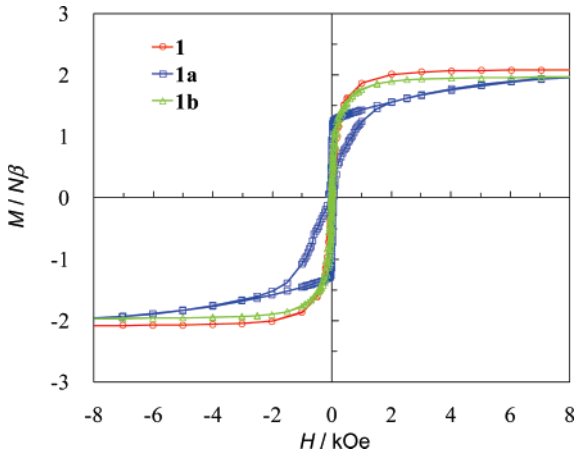


***Figure 7.*** Magnetic hysteresis loops for **1** (red), **1a** (blue), and **1b** (green) at 2 K (the solid lines are for visualization).

gradients of the $M$ vs $H$ curves than the Brillouin function for $S_T = 2/2$ strongly support the ferrimagnetic ordering in these compounds.

The magnetic hysteresis loops at 2 K are given in Figure 7. The remnant magnetization and coercive field ($H_c$) of **1** are extremely small (640 emu·mol$^{-1}$ and 12 Oe, respectively), resembling those of other $Mn^{II}Cr^{III}$ compounds.[44,45] The soft-magnet type hysteresis loop must be associated with the isotropic electronic configuration of $Mn^{II}$ and $Cr^{III}$ ions. The hysteresis loop of **1a** was slightly broadened with an $H_c$ of 60 Oe by the structural change. It is notable that the hysteresis shapes of **1** and **1b** are essentially the same, which also supports the reversible magnetic change associated with the structural transformation. The small differences between **1** and **1b** in the low-field region are also reflected in the above-mentioned small structural difference.

## Conclusion

We have successfully prepared a novel guest-responsive ferrimagnetic coordination polymer, $[Mn(NNdmenH)(H_2O)][Cr(CN)_6]\cdot H_2O$ (**1**). Initially, the 2D sheet was formed with removable water and protonated NNdmen coligands in the axial positions of the $Mn^{II}$ ion. The 2D sheet of **1** showed an SCSC structural transformation to the 3D pillared-sheet framework of $[Mn(NNdmenH)][Cr(CN)_6]$ (**1a**) by elimination of the water coligands, a formation of a new Cr−CN−Mn linkage between the neighboring sheets, and shrinkage of the intersheet space. The anhydrous **1a** swiftly adsorbed two water molecules per formula unit and reconstructed the 2D sheet (**1b**), which is almost identical to **1**. Reversible structural and magnetic conversion between **1** and **1a** accompanied with generation/cleavage of Mn−N bond was also confirmed by TGA, VT-XRPD, and various magnetic results. Adsorption measurements demonstrated characteristic chemi- and physisorption processes toward water with high affinity and size selectivity of guest molecules (MeOH, EtOH, and $CH_3CN$). The cyanide-bridged CPM **1** clearly demonstrated a guest response with changing magnetic output. The simultaneous achievement of reversible structural and magnetic changes and specific chemical responsivity will open a new route to develop the environmentally responsive materials. We also believe that the flexible magnetic hosts will be evolved to a multifunction platform based on correlation between physical properties of the hosts and guests.

**Acknowledgment.** The authors thank D. Tanaka for the adsorption measurements. This work was supported by a Grant-In-Aid for Science Research in a Priority Area "Chemistry of Coordination Space (No. 16074209)", a Grant-In-Aid for Scientific Research Program (No. 18750046), and CREST/JST programme from the Ministry of Education, Culture, Sports, Science and Technology of Japan. W.K. is grateful to JSPS Research Fellowships for Young Scientists.

**Supporting Information Available:** Photo of crystals; Dubinin-Raduskevich plot of $H_2O$ adsorption data; weak-field magnetization data, AC magnetic responses and $M$ *vs* $H$ curves of **1**, **1a**, and **1b**. X-ray crystallographic data of **1** and **1a** as CIF. This material is available free of charge via the Internet at http://pubs.acs.org.

JA074915Q